Algal Research 95 (2026) 104600

Contents lists available at ScienceDirect

Algal Research

journal homepage: www.elsevier.com/locate/algal

Nutrient deprivation stimulates soluble extracellular polymeric substances: physiological and biochemical responses in the cyanobacterium *Cyanocohniella rudolphia*

Filipa Rodrigues [a,b], Ivana Mendonça [a,b,c], Marisa Faria [a,b], Karine Mougin [d], Juan Luis Gómez Pinchetti [e], Artur Ferreira [c], Nereida Cordeiro [a,b,*]

[a] LB3, Faculty of Science and Engineering, University of Madeira, 9020-105, Funchal, Portugal
[b] CIIMAR, Interdisciplinary Centre of Marine and Environmental Research, University of Porto, 4450-208, Matosinhos, Portugal
[c] CICECO, Aveiro Institute of Materials and Águeda School of Technology and Management, University of Aveiro, 3754-909, Águeda, Portugal
[d] Université de Haute-Alsace, FST Chimie renforcée, 68100, Mulhouse, France
[e] Spanish Bank of Algae, Institute of Oceanography and Global Change (IOCAG), University of Las Palmas de G.C, Muelle de Taliarte S/N, Telde, 35214, Las Palmas, Canary Islands, Spain

ARTICLE INFO

Keywords:
Cyanocohniella rudolphia
Soluble EPS (S-EPS)
Nutrient deprivation
Starvation phase
Viscosity proxy
Spent-medium valorisation

ABSTRACT

The effect of macro- and micronutrient deprivation on the cyanobacterium *Cyanocohniella rudolphia* (BEA 0786B) over 180 days (without medium renewal) was evaluated to intensify the production of soluble extracellular polymeric substances (S-EPS). Growth, pH, cell-free medium viscosity, S-EPS content (phenol-sulfuric acid assay), Alcian Blue staining, and biochemical/structural markers were monitored to assess EPS release and extracellular matrix dynamics. Progressive nutrient depletion induced a shift from biomass growth toward extracellular-matrix investment. Microcolony formation observed around day 45 preceded a sustained high-production phase, with pronounced matrix densification evident by approximately day 75. Apparent viscosity increased in parallel with S-EPS accumulation and showed a strong correlation with extracellular carbohydrate concentration ($R^2 = 0.86$), supporting its use as an operational, non-destructive proxy for S-EPS. Alcian Blue staining qualitatively confirmed the presence of acidic polysaccharides. Quantitatively, S-EPS concentrations increased from 0.1 to 0.8 g L^{-1}, accompanied by an increase in apparent viscosity from 24.7 to 34.7 mPa·s. Morphological and spectroscopic analyses indicated a predominantly carbohydrate-rich extracellular matrix with an increasing protein contribution over time.

As an exploratory proof of concept, unprocessed S-EPS present in the spent culture medium enabled LAP-initiated photochemical formation of Au and Ag nanoparticles at 365 nm, with S-EPS acting as a stabilising and co-reducing matrix and conferring pH-responsive optical behaviour. This indicates a practical route toward integration into EPS-rich matrices to engineer stimuli-responsive coatings and biomaterials. Overall, this study demonstrates that prolonged nutrient deprivation without medium renewal is an effective strategy to intensify S-EPS accumulation in *C. rudolphia* and that apparent viscosity provides a practical in-process parameter for monitoring production and supporting direct valorisation of spent culture medium in saline bioprocesses.

1. Introduction

Cyanobacteria are ancient oxygenic phototrophs that inhabit freshwater, marine, soil, and lithic environments as unicells, colonies, or filaments, playing key roles in global carbon and nitrogen cycling [1,2]. As primary producers, they contribute substantially to ecosystem functioning and biogeochemical stability, while their physiological plasticity enables growth under a wide range of environmental conditions, including high salinity, nutrient limitation, and fluctuating light regimes. Beyond their ecological relevance, cyanobacterial biomass has emerged as a valuable resource for biotechnological applications due to its capacity to convert light, CO_2, and inorganic nutrients into biomass and extracellular products under comparatively low-input cultivation conditions [3,4].

* Corresponding author at: LB3, Faculty of Science and Engineering, University of Madeira, 9020-105, Funchal, Portugal.
E-mail address: ncordeiro@staff.uma.pt (N. Cordeiro).

https://doi.org/10.1016/j.algal.2026.104600
Received 1 October 2025; Received in revised form 16 February 2026; Accepted 17 February 2026
Available online 21 February 2026

Over the last decade, cyanobacteria have attracted increasing interest for the production of a wide range of metabolites, including pigments (*e.g.* phycobiliproteins and carotenoids), proteins, bioactive compounds, and polymeric substances, with applications in food, health, cosmetics, energy, and environmental technologies [3,4]. Their metabolic versatility and robustness position cyanobacteria as promising phototrophic cell factories within the emerging bioeconomy, particularly for processes that benefit from stress tolerance and minimal resource inputs.

Among cyanobacterial products, extracellular polymeric substances (EPS) constitute a particularly relevant class of biomolecules. EPS are heterogeneous macromolecules composed mainly of polysaccharides, often associated with proteins, lipids, and functional groups such as sulfate or carboxyl moieties, which collectively determine their rheological, interfacial, and binding properties [5,6]. EPS fulfil essential ecological functions in cyanobacteria, including protection against desiccation, ultraviolet radiation, and oxidative stress, as well as mediation of cell aggregation, surface adhesion, and biofilm formation [5–7]. From an applied perspective, these physicochemical properties underpin growing interest in cyanobacterial EPS for applications in environmental remediation, saline formulations, and biomaterials [5,6,8].

For practical purposes, EPS are commonly divided into cell-bound EPS (B-EPS), which remain associated with the cell surface, and soluble or released EPS (S-EPS), which accumulate in the surrounding culture medium [5,6]. While B-EPS have been extensively studied, S-EPS offer distinct bioprocess advantages, as they can be recovered directly from cell-free supernatants with potentially reduced downstream processing, lower solvent use and energy demand, and minimal cell disruption. Despite this potential, S-EPS remain comparatively underexplored, particularly in long-term cultivation systems.

Nutrient availability is a key factor governing cyanobacterial metabolism and carbon allocation. Under conditions of macro- or micronutrient limitation, cyanobacteria commonly undergo metabolic reprogramming in which growth and protein synthesis are constrained, while photosynthetically fixed carbon is redirected toward storage compounds and extracellular polysaccharides, a phenomenon often described as carbon overflow [5,7]. This stress-driven reallocation supports extracellular matrix development and may contribute to microenvironment stabilisation, including effects on pH and ionic conditions, as reported for EPS-rich matrices [5–7]. EPS production has been reported under nitrogen (N), phosphorus (P), or combined nutrient deprivation in several cyanobacterial genera, frequently accompanied by changes in pigment composition, extracellular architecture, and medium rheology [8–11]. However, most available studies focus on short-term batch cultures or abrupt nutrient shifts, providing limited insight into the long-term dynamics of S-EPS accumulation under sustained deprivation.

Beyond nutrient availability, cyanobacterial EPS quantity and composition are also modulated by operational factors such as salinity/ionic strength, irradiance/photoperiod, temperature, CO_2 supply and gas exchange, and hydrodynamics (shear), with strain-specific responses reported across cultivation regimes. Accordingly, EPS intensification has commonly relied on one-factor-at-a-time screening or multivariate optimisation approaches to capture interacting nutritional and operational drivers. Recent RSM/CCD optimisation using *C. rudolphia* (BEA 0786B) confirmed that deliberate modulation of N and P availability in Spirulina medium significantly affects S-EPS titres over short production windows (1–7 days) [12].

Prolonged cultivation without medium renewal represents a relevant yet underexplored strategy to induce progressive nutrient depletion while maintaining low operational inputs. Under such conditions, cultures transition gradually from fresh working-medium conditions (day-0 baseline) to limitation and starvation, offering a unique framework to investigate the temporal coupling between physiological stress, extracellular matrix development, and S-EPS production. Identifying simple, non-destructive parameters capable of tracking these transitions remains a key challenge for process implementation and scale-up.

This study addresses these gaps using the marine cyanobacterium *Cyanocohniella rudolphia* P. Jung, V. Sommer, U. Karsten & Lakatos (BEA 0786B). By monitoring growth, pH, photosynthetic pigments, extracellular proteins, apparent viscosity of the cell-free medium, and S-EPS accumulation over 180 days without medium renewal, the work aims to *(i)* characterise long-term S-EPS production dynamics under progressive macro- and micronutrient deprivation; *(ii)* link physiological stress responses with extracellular matrix development; and *(iii)* evaluate apparent viscosity as a practical in-process proxy for S-EPS accumulation in saline cyanobacterial cultures. By adopting a long-term, process-oriented approach and focusing on the recovery of soluble EPS from spent medium, this study provides new insights into deprivation-driven extracellular biopolymer production and supports the positioning of *C. rudolphia* as an emerging candidate cyanobacterial platform for low-input bioprocess strategies.

2. Methods

2.1. Strain and culture conditions

The marine cyanobacterium *Cyanocohniella rudolphia* P. Jung, V. Sommer, U. Karsten & Lakatos (BEA 0786B) was isolated from the Añana Saltworks (Álava, Spain) by the Spanish Bank of Algae (BEA-Banco Español de Algas), where it was also identified and curated. Pre-cultures were grown in Spirulina medium at 10% (v/v) (*i.e.*, a 1:10 dilution of the Spirulina medium composition described in ES1) at 30 ± 2 °C under a 10:14 h light:dark photoperiod provided by cool-white fluorescent lamps (OSRAM L 18 W/840). Photosynthetically active radiation (PAR) was measured using a HOBO® Pendant® MX2202 quantum sensor and maintained at 40 μmol photons m^{-2} s^{-1} at the level of the culture flasks inside an Aralab CP500 growth chamber, ensuring uniform illumination across replicates [12]. All solutions were prepared using ultrapure water.

2.2. Cultivation and sampling

Pre-cultures were grown in Spirulina medium diluted to 10% (v/v) to the stationary phase. Working cultures were then initiated by inoculating 25% (v/v) of a stationary-phase pre-culture into 75% (v/v) fresh Spirulina medium (10% (v/v)) (1:3, inoculum:fresh medium) to an initial OD_{750} of 0.05. Aliquots (200 mL) were maintained in 250 mL Erlenmeyer flasks (flask photobioreactors) with aeration at 0.30 vvm (litres of air per minute per litre of liquid), cultivated for 180 days without medium renewal; manual swirling was performed once daily. Three independent flasks were prepared as biological replicates (n = 3) and each flask was sampled at all time points (repeated measures). At predefined time points (days 0, 15, 30, 45, 60, 75, and 180), cultures were sampled for growth, pH, and analytical assays. Biomass for dry weight was collected by centrifugation (20 min, 4,427 *xg*; HERMLE Z360), freeze-dried to constant mass, and stored at −20 °C. Day 0 was used as the baseline reference for all subsequent comparisons within this long-term batch regime. This study was designed as a single-condition longitudinal time-course and was not intended to quantify independent effects of specific nutrient-factor levels (*e.g.,* N/P).

2.3. Growth and pH measurements

Growth rates were calculated as ln-based interval estimates between consecutive predefined sampling points and are reported as descriptive interval metrics of culture dynamics. Two interval rates were determined: μ_1 from optical density (OD_{750}) and μ_2 as a biomass production rate from dry biomass concentration (DW, $g{\cdot}L^{-1}$). For each interval, μ_1 was calculated as:

$$\mu_1\left(\text{day}^{-1}\right) = \frac{\ln(OD_{t_2}) - \ln(OD_{t_1})}{t_2 - t_1} \quad (1)$$

and μ_2 was calculated as:

$$\mu_2\left(\text{g L}^{-1}\ \text{day}^{-1}\right) = \frac{DW_2 - DW_1}{t_2 - t_1} \quad (2)$$

where OD_{t1}/OD_{t2} (or DW_1/DW_2) are the values at times t_1 and t_2 (days). Sampling points used for these interval estimates were days 0, 15, 30, 45, 60, 75, and 180. No mechanistic growth model was fitted. Optical density was measured at 750 nm (OD_{750}) using a UV-6300PC double-beam spectrophotometer, and dry biomass concentration was determined gravimetrically. pH was recorded with a Consort C5020 multi-parameter analyser.

2.4. Sample preparation

For all supernatant-based assays, samples were centrifuged (12,100 *xg* for 4 min at room temperature) to obtain the cell-free supernatant. The presence of residual cells in the supernatant was checked by microscopy (Leica DM2700 microscope equipped with a Leica DFC450 C digital camera and CoolLED pE-300 lite illumination). When residual cells were observed (from day 45 onwards), the supernatant was additionally filtered through a 0.22 μm membrane to ensure complete cell removal before extracellular assays. To verify that this filtration step did not affect S-EPS and protein quantification, a comparison was performed at day 30 using supernatants processed with and without 0.22 μm filtration; no statistically significant differences were observed ($p > 0.05$).

2.5. Apparent viscosity of cell-free supernatants

Bulk viscosity was measured at 25 °C on a Brookfield DV-III Ultra (spindle #2, 250 rpm). Each sample equilibrated for 5 min before reading; three consecutive readings were averaged. Because EPS solutions are non-Newtonian, apparent viscosity (η_{app}) is reported under the specified instrument conditions (25 °C; DV-III Ultra; spindle #2; 250 rpm).

2.6. Soluble extracellular carbohydrates quantification

A modification of the phenol-sulfuric acid method [13] was used to quantify extracellular carbohydrates in cell-free supernatants. Briefly, 1.0 mL sample was mixed with 0.5 mL 5% (w/v) phenol; 2.5 mL conc. H_2SO_4 was added rapidly, allowed to react for 10 min, vortexed, and developed for 20 min in a water bath maintained at 25 °C. Absorbance was measured at 490 nm (OD_{490}) in a quartz cuvette (1 cm path length) using a UV-6300PC double-beam spectrophotometer. A calibration curve was prepared using D-glucose (500 mg L^{-1} stock) diluted to 5–150 mg L^{-1} (linear fit, $R^2 = 0.9992$; Fig. S1). Results were expressed as glucose equivalents (mg L^{-1}). Matrix blanks (fresh medium) and reagent blanks were also included. Measurements were carried out as technical triplicates.

2.7. Extracellular protein quantification

Proteins in cell-free supernatants were measured by the Lowry method [14] with minor modifications. Reagent A (2% Na_2CO_3 in 0.1 N NaOH) was mixed with reagent B (1% sodium citrate in 0.5% $CuSO_4$) at 50:1 to give reagent C; reagent C was diluted 1:1 immediately before use. In glass tubes, 500 μL of the sample was mixed with 2.5 mL of reagent C, incubated for 10 min, and then 250 μL of diluted Folin-Ciocalteu was added. The mixture was vortexed and incubated for 30 min in a thermostated water bath at 25 °C, protected from light. The absorbance was measured at 750 nm. BSA 5 mg mL^{-1} stock diluted to 10–2000 μg mL^{-1} ($R^2 = 0.9971$) was used as standard (Fig. S2). Samples with absorbance values outside the linear calibration range were diluted and re-analysed. Results were expressed as BSA equivalents (mg L^{-1} BSA-eq). Reagent and matrix blanks were also included. Measurements were carried out as technical triplicates.

2.8. Photosynthetic pigments determination

The extraction of photosynthetic pigments was performed using the method described by Lichtenthaler [15]. Pellets from 5 mL culture (12,100 *xg*, 4 min) were resuspended in 5 mL 90% methanol, sonicated 5 min, incubated 24 h at 4 °C (dark), and clarified (12,100 *xg*, 4 min). Absorbance was measured at 470, 652, and 665 nm (baseline-corrected at 750 nm). Concentrations (μg mL^{-1}) of chlorophyll *a* (*Chl-a*), chlorophyll *b* (*Chl-b*), and total carotenoids (*Car-t*) were calculated by Eqs. (3)–(5) [15]:

$$\text{chl-}a = 16.82\ A_{665} - 9.28\ A_{652} \quad (3)$$

$$\text{chl} - \text{b} = 36.92\ A_{652} - 16.54\ A_{665} \quad (4)$$

$$\text{car} - \text{t} = \frac{1000\ A_{470} - 1.91\ \text{chl} - \text{a} - 95.15\ \text{chl} - \text{b}}{225} \quad (5)$$

The results are also presented as pigment content per dry biomass (% DW). The values are derived from the Lichtenthaler [15] equations, taking into account the extraction volume and the dry biomass weight of the pellet corresponding to the same time period.

2.9. Detection of S-EPS by Alcian Blue

S-EPS production during the experimental period was tracked, following the method described by Inoue-Sakamoto et al. [16], with minor modifications. Cell cultures were mixed in a 1:1 ratio with 1% (w/v) Alcian Blue 8GX prepared in 3% (v/v) acetic acid (pH 2.5) and incubated for 30 min at room temperature. An aliquot of 100 μL of the stained suspension was then mounted on glass slides and examined under a Leica DM2700 microscope equipped with a Leica DFC450 C digital camera and CoolLED pE-300 lite illumination. Fresh medium and dye-only blanks were processed identically as negative controls. Imaging parameters (brightness, exposure, and magnification) were kept constant across samples, and scale bars were applied uniformly. This assay was used for qualitative analysis of acidic S-EPS and was not used for quantitative S-EPS determination. Alcian Blue staining was performed at pH 2.5, which promotes binding to sulfated and carboxylated polysaccharides.

2.10. S-EPS extraction and purification

Cell-free supernatants were concentrated and desalted by ultrafiltration (Vivaflow 50R; 10 kDa MWCO; Sartorius) until the permeate conductivity reached a constant level [12]. The retentate (EPS solution) was freeze-dried, weighed to a constant mass, quantified by gravimetry, and stored at −20 °C.

2.11. Structural characterisation

2.11.1. Attenuated total reflection-Fourier transform infrared spectroscopy (ATR-FTIR)

ATR-FTIR spectra of dried biomass and UF-purified S-EPS were recorded on a PerkinElmer Spectrum BX with a single-bounce Golden Gate diamond ATR cell (DurasamplIR II, Smiths Detection, UK). Samples were dried in an oven at 40 °C before analysis to remove residual moisture. Spectra were recorded from 4000 to 700 cm^{-1}, with a resolution of 1 cm^{-1}, and a total of 32 accumulation scans were performed to enhance the spectra quality. Spectral acquisition and processing followed standard approaches commonly used for microalgal/

cyanobacterial biomass characterisation [17,18].

2.11.2. Scanning electron microscopy (SEM)

Surface micrographs were obtained by SEM using a Hitachi SU-70 HR-FESEM operated at 4 kV (field-emission mode). Cells were fixed in 2.5% (w/v) glutaraldehyde in 0.1 M sodium phosphate buffer (pH 7.2) overnight at 4 °C, washed twice with the same buffer, and dehydrated through a graded ethanol series (30, 50, 70, 90, 100% v/v). Samples were then freeze-dried, mounted on stainless-steel stubs, and carbon-coated using an Emitech K950X turbo evaporator before imaging [12].

2.11.3. Elemental analysis

The carbon, hydrogen, nitrogen, and sulfur (CHNS) contents were determined by elemental microanalysis using a LECO TruSpec CHNS analyser, with primary combustion at 1075 °C and an afterburner at 850 °C. Detection was by infrared absorption and thermal conductivity, according to the instrument configuration. Calibration was performed using methionine as the standard due to its well-defined C, H, N, and S elemental composition, making it a suitable calibration reference for CHNS analysis. Ash content (% inorganic residue) was obtained by thermogravimetric analysis (TGA) as the residual mass at 550 °C (SETSYS Setaram TGA analyser, platinum crucible), after heating freeze-dried samples from ambient temperature to 550 °C at 10 °C·min^{-1} under a 20 mL·min^{-1} oxygen flow. Sulfur was below the limit of quantification in all samples; therefore, % S was set to 0 for the oxygen-by-difference calculation. Oxygen was calculated as % O = 100 − (% C + % H + % N + % ash). The elemental and thermal analysis workflow followed standard approaches commonly applied to microalgal/cyanobacterial biomass characterisation [18].

2.12. Plasmonic nanoparticles synthesis and environmental responsiveness

S-EPS-metal salt mixtures were exposed to UV light (λ = 365 nm; LED source; 5 cm sample-lamp distance; irradiance of 10 mW·cm^{-2}) in the presence of LAP photoinitiator for 10 min under gentle stirring at room temperature, enabling *in situ* photoreduction to plasmonic Au/Ag nanoparticles. To assess environmental responsiveness, S-EPS-NP systems were challenged with varying pH levels. Acidification (pH ≤ 4) and alkalinisation (pH > 8) were performed using HCl (1.0 M) and NaOH (1.0 M), respectively. Changes in colloidal stability and optical properties were monitored by UV–Vis spectroscopy (UV-6300PC spectrophotometer) to confirm surface plasmon resonance (SPR) bands, and by transmission electron microscopy (TEM; Philips/FEI Tecnai-12 with TVIPS F224 CCD camera; 80–120 kV) to assess particle morphology, size, and structural features.

2.13. Statistical analysis

Statistical analysis was performed in GraphPad Prism 8.0.2. Data are reported as the mean ± SD of three independent biological replicates (n = 3; independent culture flasks sampled over time; repeated-measures design). Each assay was performed in technical triplicate. Normality was assessed with the D'Agostino-Pearson test (α = 0.05). Time-course comparisons were analysed using one-way repeated-measures ANOVA followed by Tukey's multiple-comparisons test; different letters in figures indicate significant differences ($p < 0.05$). For two-group comparisons, unpaired two-tailed *t*-tests were used.

3. Results and discussion

3.1. Culture dynamics under nutrient deprivation

Nutrient concentrations were not directly quantified during the 180-day cultivation period. Instead, nutrient stress developed progressively as a consequence of cellular uptake in the absence of medium renewal and was inferred from coordinated physiological, biochemical, and extracellular responses.

Under sustained nutrient deprivation, *C. rudolphia* exhibited clear changes in growth and physiology over 180 days. OD_{750} and dry biomass (Fig. 1A), derived growth rates μ_1 and μ_2 (Fig. 1B), and pH (Fig. 1C) illustrate these dynamics. Growth followed a non-classical pattern: an initial phase of progressively increasing nutrient limitation, driven by nutrient uptake without medium renewal, persisted until approximately days 60–75. Thereafter, both OD_{750} and dry biomass declined, consistent with a transition into starvation-like physiology inferred from the convergence of multiple indicators (μ_1/μ_2 trends, OD-DW divergence, pH maximum, and microcolony/matrix development), rather than from a predefined depletion time (Fig. 1A,B). Apparent growth rates (μ_1 and μ_2), calculated as described in Section 2.3, reflect the progressive loss of growth capacity during long-term cultivation under nutrient depletion. The divergence between rising OD_{750} and falling dry biomass was quantitatively supported by a weak correlation between OD_{750} and dry biomass ($R^2 = 0.39$; Fig. S3), and likely reflects shifts in cellular composition and investment in the extracellular matrix (including S-EPS) under stress, rather than accurate biomass accrual [19,20]. Microscopy indicated microcolony formation from day 45, aligning with the subsequent depression of μ_1/μ_2 and the S-EPS-centred analyses presented below. Across time, OD_{750}, dry biomass, μ_1, μ_2 and pH differed significantly (Fig. 1).

These variables were not analysed as independent drivers but as integrative indicators of the culture's physiological state. Accordingly, all interpretations are made relative to the day-0 baseline (fresh working medium; Spirulina 10% v/v) within this long-term batch regime. Their coordinated temporal behaviour reflects a system-level transition from day-0 baseline conditions toward nutrient limitation and starvation, which provides the framework for interpreting the subsequent extracellular matrix development and S-EPS accumulation. Such non-classical batch behaviour under nutrient stress is widely documented in cyanobacteria, where limitation of N, P, or essential micronutrients constrains protein synthesis and cell division, leading to reduced biomass accumulation and altered carbon allocation [21,22]. Similar growth attenuation under nutrient deprivation has been reported for several cyanobacterial genera, including *Synechocystis*, *Nostoc*, and *Anabaena*, and is commonly associated with a metabolic shift from growth-oriented pathways toward stress acclimation and survival [6,8].

In this study, pH increased steadily to 10.3 by day 75 and then declined to 9.7 by day 180, coinciding with culture decline. This trajectory is consistent with an early phase dominated by photosynthetic alkalinisation under deprivation, followed by reduced photosynthetic activity and increased respiratory/mineralisation processes as deprivation progressed toward starvation. The timing aligns with microcolony formation (day 45) and the subsequent intensification of S-EPS release, as inferred from apparent viscosity and colorimetric read-outs. Because cyanobacterial polysaccharides behave as polyelectrolytes, pH modulates polymer charge density and hydrodynamic volume and, therefore, apparent viscosity; viscosity was measured at constant temperature and interpreted within the observed pH window (9.7–10.3), while S-EPS colorimetry was conducted at fixed assay pH (Alcian Blue at pH 2.5) to decouple analytical conditions from culture pH. The rise in pH to 10 by day 75 is also consistent with the literature, in which alkaline conditions, especially when combined with N deprivation, reallocate metabolism away from growth machinery (chlorophyll/protein) and toward storage/extracellular outputs [9,10].

Progressive nutrient depletion imposes a metabolic constraint on biomass synthesis, leading to declining growth rates and biomass loss. Under these conditions, photosynthetically fixed carbon cannot be efficiently channelled into growth-related pathways and is increasingly redirected toward extracellular polysaccharide production, consistent with a carbon overflow response. This metabolic reallocation explains the inverse relationship observed between declining μ values and increasing S-EPS accumulation, as well as the concomitant development

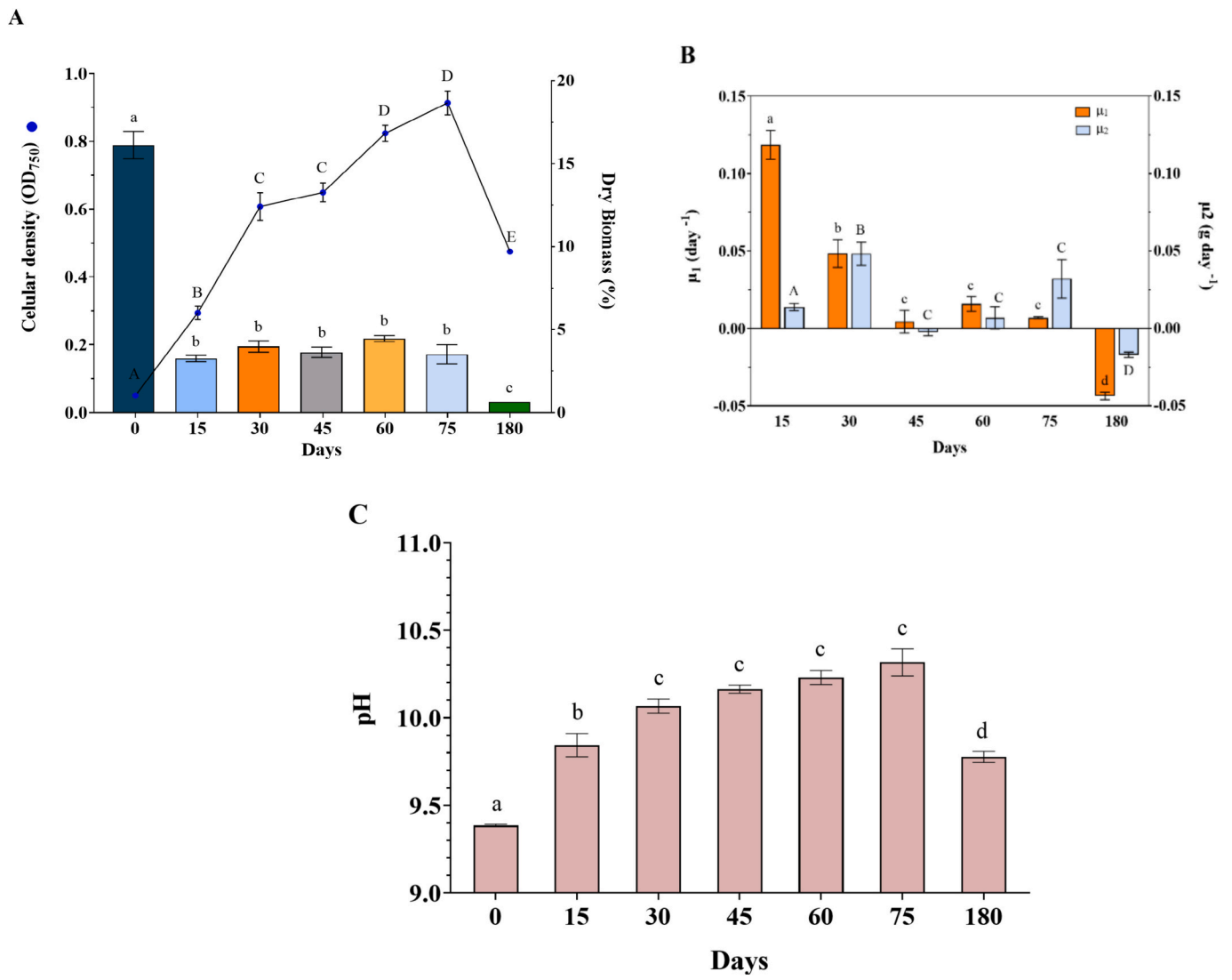

Fig. 1. Growth and physiological parameters of *C. rudolphia* under nutrient deprivation over 180 days. (**A**) Optical density and dry biomass. (**B**) Average specific growth rate (μ_1) and biomass production rate (μ_2). (**C**) Culture pH. Data represent mean ± SD (n = 3). Different letters denote significant differences in means among time points ($p < 0.05$).

of a dense extracellular matrix during the nutrient-stress phase.

The experimental design was conceived to investigate long-term, deprivation-driven metabolic reprogramming under batch cultivation without medium renewal, rather than nutrient-specific uptake kinetics. Although direct measurements of individual nutrient concentrations were not included, future studies integrating nutrient profiling with these process-level markers will be valuable to quantitatively link nutrient depletion dynamics with extracellular polymer production.

3.2. S-EPS dynamics and apparent viscosity

Soluble extracellular carbohydrates in the cell-free supernatant, quantified by the phenol-sulfuric acid assay (expressed as glucose equivalents), increased throughout the 180 days of nutrient deprivation (Fig. 2A). An early rise was evident by day 15, followed by continued accumulation across subsequent time points. A transient stabilisation between days 30 and 45 suggests a short-lived plateau before renewed accumulation. Overall, this trajectory supports sustained extracellular investment during prolonged deprivation, consistent with an adaptive strategy to long-term deprivation: accumulation of S-EPS supports *(i)* protection from oxidative/physical stress *via* a hydrated polyelectrolyte matrix, *(ii)* microenvironment control around microcolonies (buffering and ionic strength), and *(iii)* rheological modification of the medium captured by the concomitant rise in apparent viscosity [8]. The pattern aligns with metabolic reprogramming under deprivation, with preferential channelling of fixed carbon to carbohydrate biosynthesis and extracellular matrix formation rather than biomass accrual.

To test whether apparent viscosity tracks S-EPS accumulation, apparent viscosity (η_{app}) of the cell-free medium at 25 °C was monitored in parallel with downstream S-EPS yield (UF/lyo; g L^{-1}). η_{app} increased stepwise from day 15 to day 75 and then remained at a high level at day 180 (no additional increase relative to day 75; Fig. 2), whereas S-EPS yield continued to increase to day 180. Taken together, these data show a positive association between η_{app} and S-EPS under nutrient deprivation: η_{app} captures the onset and plateau of the rheological response, while S-EPS continues to accumulate. Mechanistically, the rise in viscosity is consistent with increasing concentrations of hydrated, high-molecular-weight polysaccharides in the medium, whose hydrodynamic volume and chain entanglement contribute to higher η_{app} at the imposed shear [5,6]. The timing aligns with other markers, including microcolony formation (day 45) and an alkaline pH maximum (day 75). It coincides with the increase in extracellular carbohydrates (Fig. 2A), supporting a coordinated shift from growth to extracellular-matrix investment as cultures transition from nutrient limitation to starvation

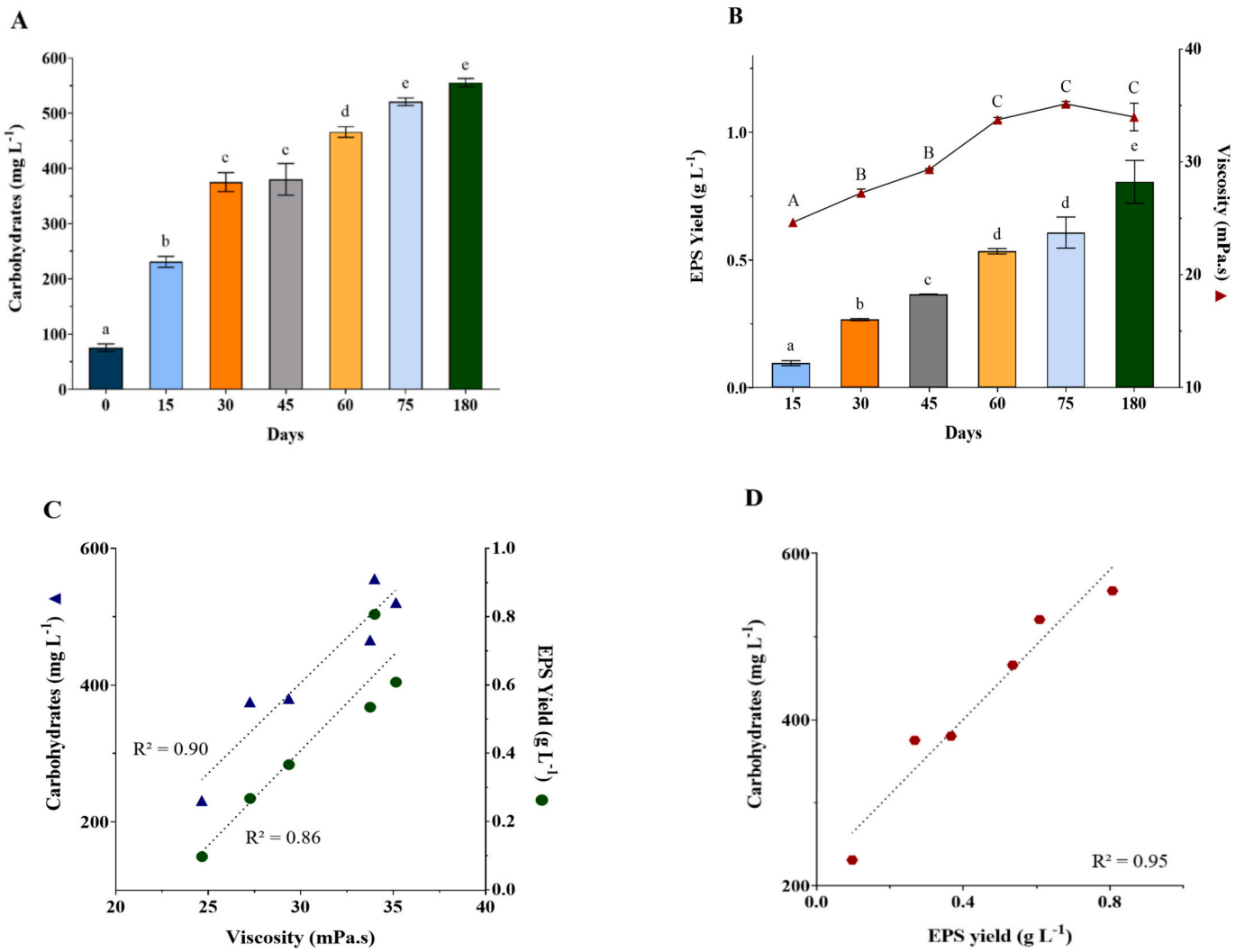

Fig. 2. **(A)** Extracellular total carbohydrates of *C. rudolphia* (mg L^{-1}; glucose equivalents) over 180 days under nutrient deprivation, mean ± SD (n = 3). **(B)** Apparent viscosity and S-EPS yield for *C. rudolphia* over 180 days. **(C)** Correlations of η_{app} with extracellular carbohydrates and with S-EPS yield. **(D)** Correlation between extracellular carbohydrates and S-EPS yield. Distinct letters denote significantly different means among time points ($p < 0.05$).

[7,19,20]. The viscosity-S-EPS relationship was quantified by ordinary least-squares regression (based on the predefined sampling points), with η_{app} correlating with UF/lyo S-EPS yield ($R^2 = 0.86$; Fig. 2C) and with phenol-sulfuric carbohydrates ($R^2 = 0.90$; Fig. 2C). Operationally, these results support a practical harvest window spanning days 60–180, when ηapp is high and shows no significant change among late time points ($p > 0.05$; Fig. 2B), while S-EPS yield continues to rise.

Enhanced accumulation of soluble EPS under nutrient deprivation is consistent with a stress-driven metabolic reprogramming commonly reported for cyanobacteria. When growth-related sinks are constrained by nutrient limitation, photosynthetically fixed carbon is increasingly redirected toward extracellular polysaccharide synthesis, a response often described as carbon overflow [5–7]. This reallocation supports both metabolic balance and the development of a protective extracellular matrix.

Previous studies have shown that short-term N or P limitation can stimulate EPS production in cyanobacterial genera such as *Nostoc*, *Phormidium*, and *Cyanothece*; however, these studies typically rely on abrupt nutrient shifts or relatively short cultivation periods [6,8]. In contrast, the present work demonstrates that prolonged, progressive nutrient deprivation without medium renewal sustains S-EPS accumulation over extended time scales, defining a stable late-phase regime that is not captured in short-term experiments.

These long-term batch dynamics complement recent short-cycle RSM/CCD optimisation performed with the same strain, where controlled modulation of N and P availability in Spirulina medium significantly shifted S-EPS titres over 1–7 days. Taken together, the short-cycle optimisation results establish nutrient-responsiveness, while the present 180-day, no-renewal trajectory defines when apparent viscosity becomes a stable in-process signal, supporting trigger-based harvest under low-input operation. These approaches are complementary: factor-driven optimisation *vs.* long-term trajectory definition under low-input operation.

3.3. Cellular and biochemical responses under nutrient deprivation

Cellular and extracellular read-outs were examined to contextualize the rheological shift observed under deprivation. Bright-field and Alcian Blue microscopy captured the transition from dispersed trichomes to microcolony formation and matrix densification, while pigments and extracellular proteins tracked metabolic reallocation consistent with S-EPS investment.

3.3.1. Microscopy

Bright-field microscopy at 0, 45, and 180 days showed typical *C. rudolphia* trichomes initially dispersed with minimal extracellular

material (Fig. 3A1). By day 45, microcolonies were evident (Fig. 3A2), and by day 180, a mucilaginous cloak had surrounded the trichomes, accompanied by visible pigment loss (Fig. 3A3), consistent with the progression from nutrient limitation to starvation. Occasional enlarged cells within trichomes were visible under bright-field microscopy (Fig. 3A1). Alcian Blue staining (pH 2.5) confirmed that the halos correspond to acidic polysaccharides. At day 0, faint pericellular sheaths consistent with bound EPS (B-EPS) were visible, and released/soluble material was scarce (Fig. 3B1). By day 45, stained aggregates bridged neighboring filaments (Fig. 3B2). At day 180, staining was intense with three-dimensional networks apparent: pericellular B-EPS (yellow arrows) and cell-independent clumps consistent with S-EPS (red arrows) (Fig. 3B3).

Scanning electron microscopy corroborated these trends. At day 0, the surfaces appeared relatively clean, with only thin fibrillar residue visible (Fig. 4). By day 180, cells were embedded in a dense fibrillar-amorphous matrix with globular deposits and sheet-like bridges between trichomes (Fig. 4). Such architecture plausibly buffers the microenvironment, retains water/ions, and mediates adhesion, supporting survival when nutrients are scarce. The morphological progression is temporally concordant with bulk measurements: extracellular carbohydrates rise steadily (Fig. 2), extracellular proteins peak by day 75 and then decline (Fig. 6), pH reaches a maximum at day 75 (Fig. 1C), and viscosity increases within the same window. Together, these observations support the progressive enrichment of the extracellular matrix and the accumulation of S-EPS from baseline through long-term deprivation.

3.3.2. *Photosynthetic pigment dynamics*

Cyanobacteria adjust their light-harvesting and photoprotective pools in response to nutrient deprivation. Chlorophylls support energy capture, whereas carotenoids dissipate excess excitation and mitigate oxidative stress [23]. Tracking pigments, therefore, provides a direct read-out of physiological adjustment. Pigment content per dry biomass (Fig. 5) showed the expected stress pattern: chlorophyll *a* (*Chl-a*) decreased toward day 60, consistent with reduced photosynthetic capacity under sustained deprivation, while total carotenoids exhibited a relative increase during the mid-to-late ageing phase, supporting a protective/photoprotective role. These trends align with the observed transition from growth to extracellular-matrix investment [24]. In contrast, chlorophyll *b* (*Chl-b*) increased from day 60 onward, consistent with the reconfiguration of the antenna to optimise spectral capture under stress. Across time points, differences in *Chl-a*, *Chl-b,* and carotenoids were significant ($p < 0.05$; Fig. 5). A positive correlation was observed between dry biomass and *Chl-a* ($R^2 = 0.74$; Fig. S3), indicating that biomass accumulation remained linked to photosynthetic pigment content under nutrient deprivation. The early carotenoid peak at day 30 coincided with the first significant rise in extracellular carbohydrates in the cell-free supernatant (Fig. 2A), and the subsequent increase in *Chl-b* from day 60 preceded the second escalation in extracellular carbohydrates (days 60–180) and the viscosity maximum around day 75, supporting a coordinated shift from growth to protection with greater investment in S-EPS and extracellular matrix. Together with the pH maximum at day 75 (Fig. 1C), these turning points mark a transition from nutrient limitation to an emerging starvation phase.

3.3.3. *Extracellular protein dynamics*

Extracellular proteins in the cell-free supernatant (BSA equivalents) increased up to day 75 and declined thereafter (Fig. 6). Differences among time points were significant ($p < 0.05$). The early rise is consistent with stress-associated secretion (adhesins, binding proteins, and *exo*-enzymes) that supports microcolony formation and matrix remodelling during nutrient limitation. The subsequent decline until day 180 aligns with the transition into starvation, where N is recycled from accumulated proteins, including those involved in metabolic activity, and extracellular proteins are lost through proteolysis, denaturation at high pH, and/or adsorption into the carbohydrate-rich S-EPS matrix. Together with the sustained increase in extracellular carbohydrates (Fig. 2A), this pattern indicates a shift to a carbohydrate-dominated S-EPS in late phases, matching the viscosity behaviour reported below.

Intra- *vs.* extracellular partitioning of proteins, carbohydrates, and pigments was not quantified in this study; therefore, a direct discrimination between active secretion and passive leakage cannot be made. However, SEM micrographs showed trichomes embedded in a structured extracellular matrix without obvious cellular debris, and the extracellular protein profile was transient (a peak at day 75 followed by a decline), which is inconsistent with extensive cell lysis as the main driver of extracellular accumulation.

Overall, these observations support an EPS-enriched milieu and motivate the structural analysis (ATR-FTIR/CHNS) presented next.

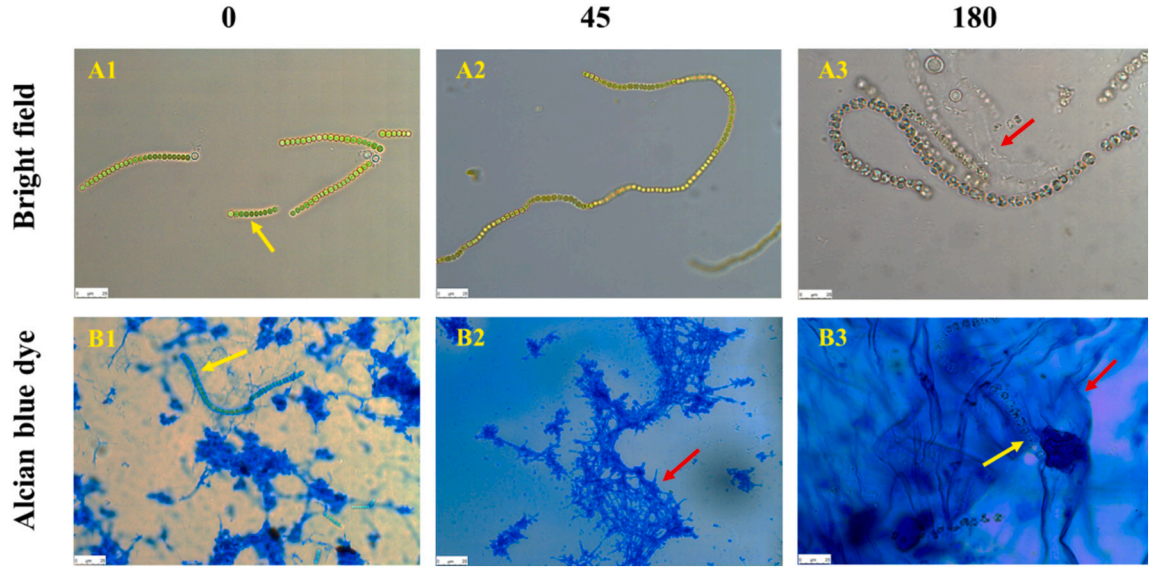

Fig. 3. Optical microscopy of *C. rudolphia* under bright-field (**A**) and culture medium stained with Alcian Blue (×400) (**B**) throughout the 180-day experimental period. Red arrows indicate S-EPS and yellow arrows indicate B-EPS. (For interpretation of the references to colour in this figure legend, the reader is referred to the web version of this article.)

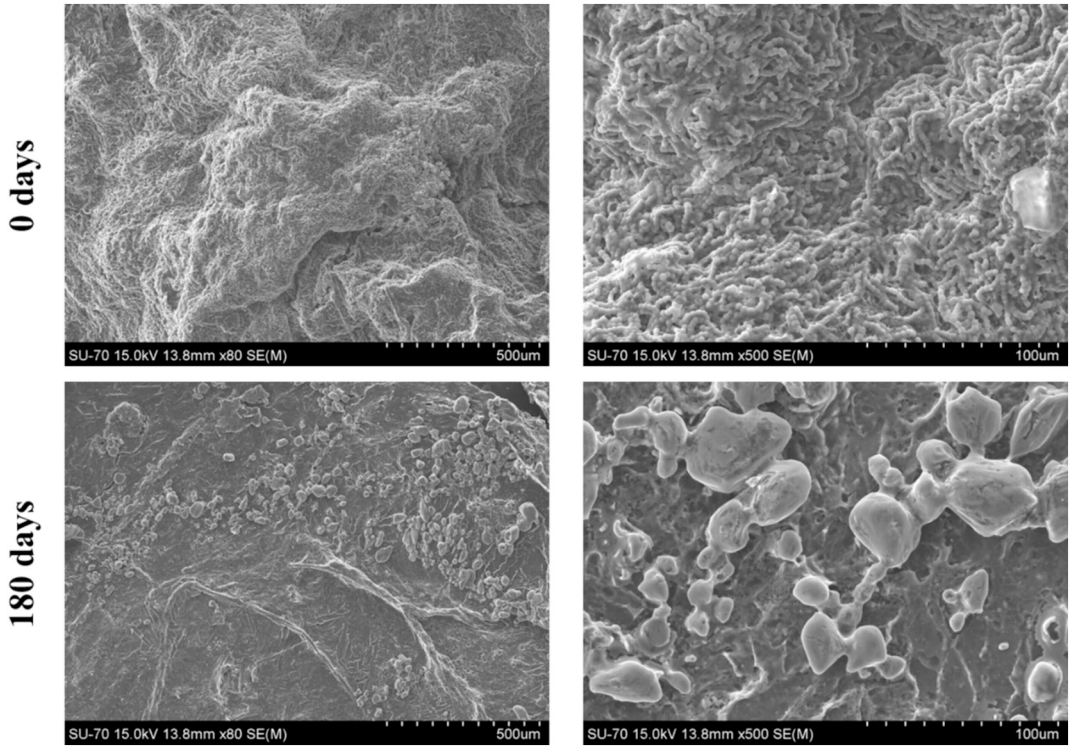

Fig. 4. Scanning electron micrographs (×80 - left and ×500 - right) of *C. rudolphia* at day 0 and day 180.

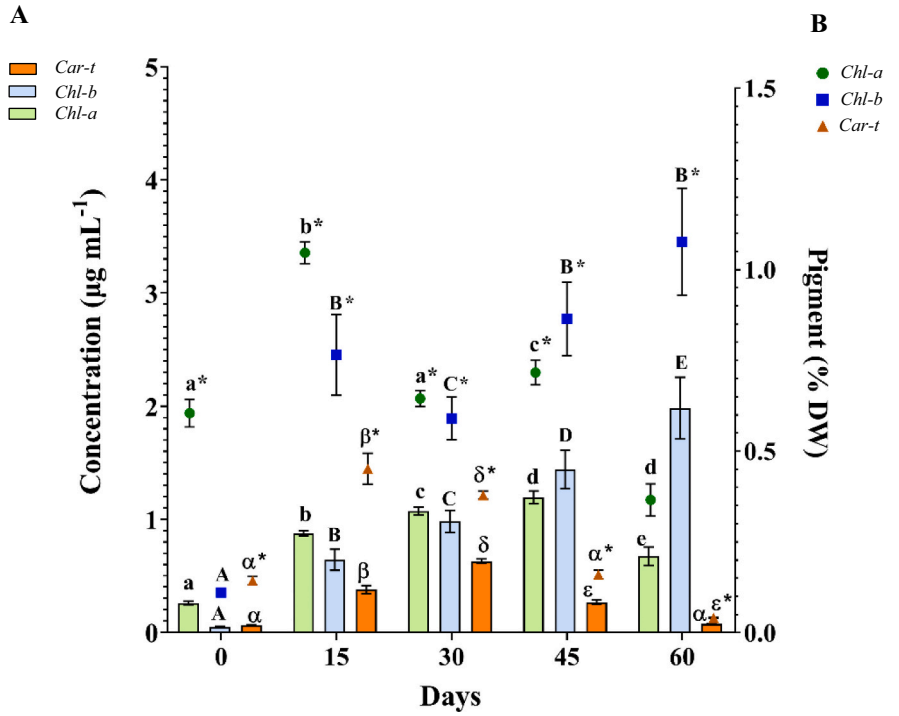

Fig. 5. Photosynthetic pigment dynamics during nutrient deprivation in *C. rudolphia*. (**A**) Pigment concentrations (µg mL^{-1}). (**B**) Pigment content normalised to dry biomass (% DW); values are means ± SD (n = 3). Distinct letters (Greek letters for carotenoids, uppercase Latin letters for *Chl-b*, and lowercase Latin letters for *Chl-a*) denote significantly different means among time points ($p < 0.05$). *Letters refer to statistical comparisons performed on panel B (% DW) only.

3.4. Structural characterisation

ATR-FTIR spectroscopy was used to characterise the biomass at representative time points (0, 45, 180 days) and the UF-purified S-EPS (Fig. 7). The aim was to follow macromolecular shifts under nutrient deprivation and to fingerprint the soluble extracellular matrix. For biomass (cells) the spectra displayed bands characteristic of hydrated polysaccharides, proteins and lipids: a broad O—H stretching band at 3200–3400 cm^{-1}, C—H stretching at 2920 and 2850 cm^{-1}, amide I and II near 1650 and 1540 cm^{-1}, respectively, and a polysaccharide

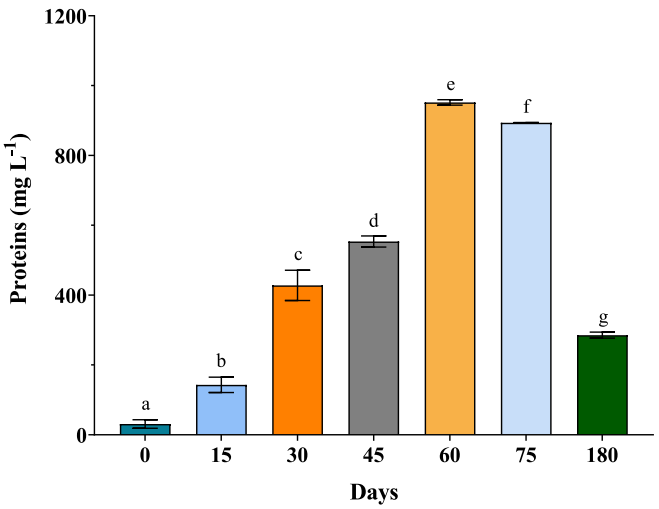

Fig. 6. Extracellular protein concentration of *C. rudolphia* (mg L^{-1}; BSA equivalents) in cell-free supernatant over 180 days under nutrient deprivation, mean ± SD (n = 3). Distinct letters denote significantly different means among time points ($p < 0.05$).

C—O—C/C—O stretching region at 1150–1000 cm^{-1} with a strong 1040 cm^{-1} pyranose band [19–21]. By day 45, reduced intensity at 3400 cm^{-1} (O—H stretching) and 1400 cm^{-1} (O—H deformation/carboxylate symmetric stretch) suggested altered hydrogen bonding/hydration of polysaccharides; in parallel, increased definition of bands around and below 900 cm^{-1} indicated enhanced contributions from glycosidic linkages/monomeric motifs [25,26]. By day 180, attenuation of the lipid-associated C═O (1750 cm^{-1}) and C—O (1100 cm^{-1}) together with more defined amide I/II bands, was consistent with a relative lipid decrease and a higher protein/polysaccharide signature [17,18].

Purified S-EPS spectra were dominated by polysaccharide bands (broad O—H 3200–3400 cm^{-1}; C—H 2920/2850 cm^{-1}; multiple features at 1150–1000 cm^{-1}, strong 1040 cm^{-1} pyranose), with amide I/II contributions (1650/1540 cm^{-1}) indicating proteinaceous components; note that 1640–1650 cm^{-1} may include bound-water bending in hydrated matrices [27–29]. The absence of a pronounced ester C═O in 1700–1770 cm^{-1} suggests low levels of esterified uronic acids/diacetyl esters [27]. Weak features near 1260 cm^{-1} are compatible with sulfate substituents.

Elemental composition of UF-purified S-EPS shifted coherently with the FTIR trends (Table 1): carbon and hydrogen increased over time, N increased more markedly, and oxygen (by difference) decreased. On a mass-percentage basis, the C:N mass ratio decreased from 34:1 (day 15) to 15:1 (day 180), indicating greater N incorporation into the extracellular matrix; O/C declined from 2.137 to 1.450, while H/C increased from 0.135 to 0.143. The drop in O/C, together with the modest rise in H/C, indicates progressive de-oxygenation (a lower average oxidation state), consistent with a higher contribution of neutral polysaccharides and/or protein relative to carboxylated/esterified moieties.

These inferences are concordant with ATR-FTIR: *(i)* intensification of the polysaccharide-associated C—O—C/C—O region (1150–1000 cm^{-1}) and a strong 1040 cm^{-1} pyranose band [30,31]; *(ii)* clearer amide I/II (1650/1540 cm^{-1}) compatible with higher proteinaceous/nitrogenous content [27,28]; and *(iii)* attenuation of lipid-associated ester C═O (1730–1750 cm^{-1}) toward late time points [17,18,32]. Because oxygen is calculated by difference, its downward trend should be interpreted cautiously; nevertheless, the combined FTIR-CHNS evidence supports a carbohydrate-dominated S-EPS with an increasing protein contribution, consistent with a denser, hydrated, polyelectrolyte matrix that buffers microenvironments, mediates adhesion, and contributes to the observed rheology under long-term deprivation [5–7].

From a physiological standpoint, under progressive nutrient limitation, biomass formation becomes constrained while photosynthetic carbon fixation can persist, favouring carbon overflow and the redirection of assimilated carbon into extracellular polysaccharides. This extracellular matrix investment (microcolony formation and matrix densification) is consistent with stress acclimation that enhances protection and local resource retention. As starvation progresses, resource redistribution and recycling, particularly N scavenging, can contribute to the observed transient extracellular-protein peak followed by a carbohydrate-dominated extracellular pool, consistent with the sustained increase in S-EPS and the apparent viscosity trajectory. Similar compositional shifts have been reported for cyanobacterial EPS under stress conditions [6,8].

3.5. *Exploratory proof-of-concept: plasmonic nanoparticles from spent-medium S-EPS*

Concept. S-EPS present in the cell-free culture medium of *C. rudolphia* can act as a green reagent for plasmonic nanoparticle formation. Under LAP-initiated 365 nm photochemical irradiation, the S-EPS matrix provides mild reducing capacity and capping/stabilising sites typical of

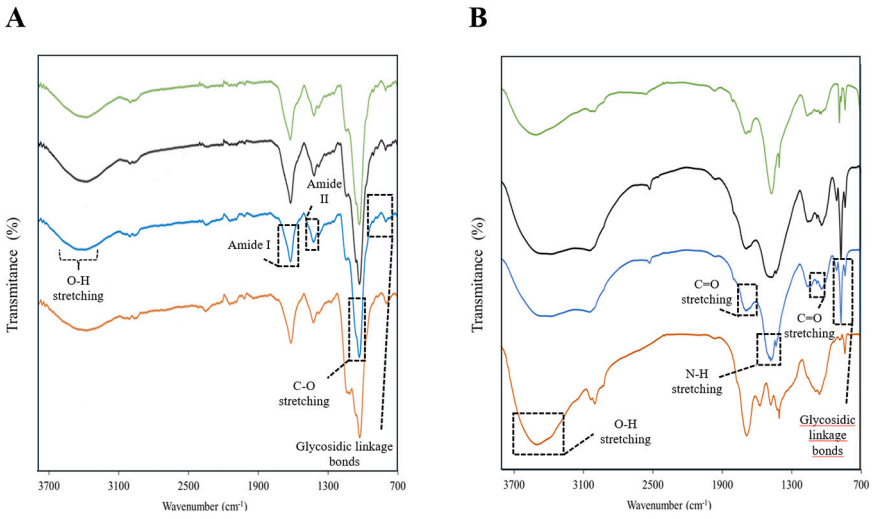

Fig. 7. ATR-FTIR spectra of *C. rudolphia*: (**A**) biomass (cells) and (**B**) UF-purified S-EPS, each at 0 (orange line), 45 (blue line), 75 (black line), and 180 days (green line). (For interpretation of the references to colour in this figure legend, the reader is referred to the web version of this article.)

Table 1
Elemental composition (wt%) and mass-based ratios of UF-purified S-EPS from *C. rudolphia* over 180 days.

Day	% C	% H	% N	% O*	H/C	O/C	C/N
15	29.329 ± 2.499[a]	3.958 ± 0.490[a]	0.855 ± 0.048[a]	62.647 ± 0.445[a]	0.135 ± 0.014[a]	2.136 ± 0.015[a]	34.303 ± 1.931[a]
30	33.211 ± 1.196[b]	4.891 ± 0.212[b]	0.637 ± 0.012[b]	58.077 ± 0.037[b]	0.147 ± 0.001[a]	1.749 ± 0.000[b]	52.137 ± 1.004[b]
45	35.631 ± 0.738[c]	4.975 ± 0.213[b]	0.818 ± 0.001[c]	55.398 ± 0.040[c]	0.140 ± 0.000[a]	1.555 ± 0.002[c]	43.559 ± 0.340[c]
60	35.548 ± 0.873[c]	4.918 ± 0.230[b]	1.019 ± 0.034[d]	55.330 ± 0.242[c]	0.138 ± 0.004[a]	1.545 ± 0.010[c]	34.885 ± 1.099[d]
75	34.763 ± 1.126[c]	5.374 ± 0.135[b]	1.741 ± 0.042[e]	54.938 ± 1.216[c]	0.155 ± 0.000[a]	1.580 ± 0.081[c]	19.967 ± 0.102[e]
180	36.422 ± 0.165[c]	5.213 ± 0.042[b]	2.354 ± 0.024[f]	52.826 ± 0.232[c]	0.143 ± 0.000[a]	1.450 ± 0.013[c]	15.472 ± 0.088[f]

* Calculated value: % O = 100 − (% C + % H + % N + % Ash (3.185%)).

polysaccharide polyelectrolytes; minor proteinaceous moieties (consistent with amide I/II bands in ATR-FTIR) may further contribute to colloidal stabilisation and redox behaviour [33,34].

Proof of concept. S-EPS from the spent, cell-free medium was used directly, *via* an environmentally benign, LAP-initiated 365 nm photochemical step, to nucleate Au and Ag nanoparticles in saline conditions. Mixing the medium with $HAuCl_4$ or $AgNO_3$ yielded Au and Ag colloids whose UV–Vis spectra showed broad localised surface-plasmon bands, indicative of polydisperse populations (Fig. 8A). For Au, the plasmon band appeared in the expected visible region and was broadened, consistent with size dispersion; for Ag, an analogue band was observed in the characteristic silver-colloid region, likewise broadened (Fig. 8A). TEM corroborated these readings, revealing irregular particle morphologies and aggregates for both metals (Fig. 8B). The suspensions were stimulus-responsive: S-EPS-AuNPs exhibited colour shifts upon acidification and alkalinisation (Fig. 8A), consistent with plasmonic-coupling changes mediated by polyelectrolyte interactions at the particle-matrix interface.

These results demonstrate the feasibility of generating optically responsive Au/Ag nanoparticles under marine-compatible conditions, illustrating a practical valorisation pathway.

3.6. Future directions

This study was designed with an applied goal: to enable the use of spent cultivation medium, typically discarded, by recovering S-EPS directly from the cell-free supernatant with low chemical input. Accordingly, biomass and its constituents were not the primary focus; biomass was monitored for productivity and pigments to relate growth cessation to the increase in S-EPS production. Demonstrating process feasibility provides an operational basis and points to three immediate avenues: *(i)* time-resolved monitoring of key nutrients (N, P) to mechanistically link medium composition, S-EPS kinetics, and process signals; *(ii)* compositional mapping of the ageing biomass to evaluate cascade co-valorisation scenarios; and *(iii)* assessment of medium adjustment/recycling and the use of alternative or surplus streams, aiming at full-cultivation utilisation within an algal biorefinery framework.

In parallel, a LAP-initiated 365-nm photochemical proof-of-concept showed that unprocessed S-EPS can yield pH-responsive Au/Ag nanoparticles (S-EPS acting as stabiliser/co-reductant), pointing to integration into EPS-rich matrices to engineer stimuli-responsive coatings and biomaterials; targeted optimisation (size distribution, colloidal stability) will support application readiness.

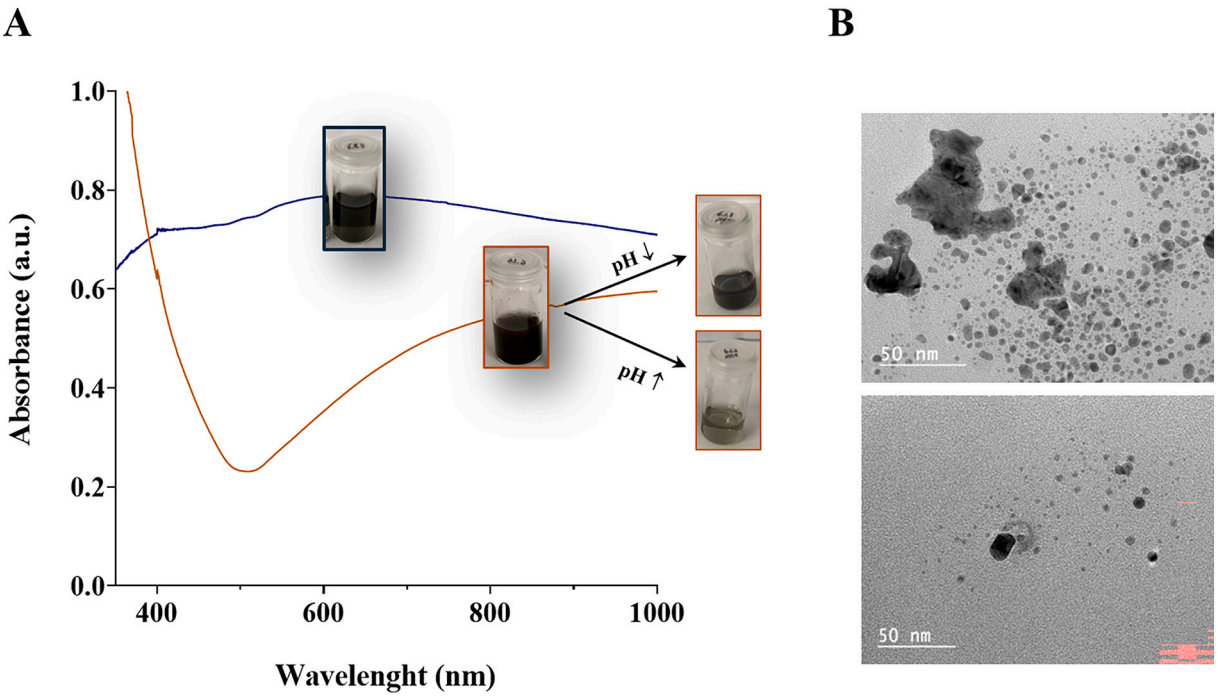

Fig. 8. LAP-initiated photochemical formation of plasmonic nanoparticles using spent-medium S-EPS from *C. rudolphia*. **(A)** UV–Vis spectra of gold (AuNPs) and silver (AgNPs) colloids. Insets: visible colour response of S-EPS-AuNPs to pH (left to right: acidified, native suspension, basified). **(B)** Transmission electron micrographs of AuNPs (left) and AgNPs (right) formed in the S-EPS matrix. (For interpretation of the references to colour in this figure legend, the reader is referred to the web version of this article.)

4. Conclusions

Prolonged nutrient deprivation shifted *C. rudolphia* (BEA 0786B) from growth to extracellular-matrix investment, enriching the culture medium in soluble EPS (S-EPS). At the physiological level, this transition is consistent with stress-driven metabolic reprogramming, whereby growth-limiting nutrient availability constrains biomass synthesis and photosynthetically fixed carbon is redirected toward extracellular polysaccharide production (carbon overflow). This reallocation provides both a metabolic sink for excess carbon and a protective extracellular matrix that supports stress acclimation, potentially contributing to pH microenvironment modulation and supporting the extracellular microenvironment. The apparent viscosity of cell-free culture medium provided a simple, non-destructive in-process proxy for S-EPS, enabling trigger-based harvest during a mid-to-late ageing phase (days 60–180) when the viscosity signal is high and stable. These findings align with stress-driven metabolic reallocation reported for microalgae/cyanobacteria and position pH-aware, low-input deprivation as a practical intensification route in which S-EPS can be monitored by apparent viscosity and recovered from spent medium with reduced chemical inputs. Direct spent-medium valorisation *via* ultrafiltration and drying delivered S-EPS without solvent precipitation, aligning with resource-efficient process design principles. The resulting marine biopolymer shows rheology and film-forming capacity compatible with saline environmental separations and other biomaterial uses where bio-based origin and salt tolerance are valued. As an exploratory adjunct, unprocessed S-EPS also enabled LAP-initiated photochemical formation of Au/Ag nanoparticles with S-EPS as a stabiliser/co-reductant, exhibiting pH-responsive optical behaviour, indicating an additional valorisation vector toward smart, biodegradable materials. Within this context, apparent viscosity offers a practical Process Analytical Technology (PAT) handle to trigger S-EPS harvest and standardise processing from spent medium. The cultivation and recovery strategy explored in this study follows low-input and solvent-minimising design principles commonly associated with resource-efficient bioprocesses. Taken together, these outcomes establish an operational basis; next steps will focus on time-resolved nutrient monitoring, compositional mapping of ageing biomass for cascade co-valorisation, and assessment of medium recycling/adjustment and alternative or surplus streams within an algal biorefinery framework.

CRediT authorship contribution statement

Filipa Rodrigues: Writing – original draft, Visualization, Investigation, Formal analysis, Data curation. **Ivana Mendonça:** Writing – original draft, Visualization, Formal analysis. **Marisa Faria:** Writing – original draft, Validation, Methodology, Investigation, Formal analysis, Data curation, Conceptualization. **Karine Mougin:** Writing – review & editing, Validation, Data curation, Conceptualization. **Juan Luis Gómez Pinchetti:** Writing – review & editing, Supervision. **Artur Ferreira:** Writing – review & editing, Supervision, Resources, Project administration. **Nereida Cordeiro:** Writing – review & editing, Validation, Supervision, Resources, Project administration, Methodology, Conceptualization.

Declaration of Generative AI and AI-assisted technologies in the writing process

During manuscript drafting, the authors used ChatGPT solely for language polishing. The authors reviewed and edited the text and are responsible for all content. No generative AI was used to create or alter figures, images, or artwork.

Declaration of competing interest

The authors declare that they have no known competing financial interests or personal relationships that could have appeared to influence the work reported in this paper.

Acknowledgements

This research was supported by the European Territorial Cooperation Programme Interreg MAC 2021–2027 through the CALYPSO project (1/MAC/1/1.1/0088). CIIMAR was funded by the Foundation for Science and Technology (FCT), through UID/04423/2025, UID/PRR/04423/2025, and LA/P/0101/2020. Filipa Rodrigues, Ivana Mendonça, and Marisa Faria were supported by FCT doctoral grants 2024.01262.BD, 2023.04389.BD, and 2020.06615.BD, respectively.

Appendix A. Supplementary data

Supplementary data to this article can be found online at https://doi.org/10.1016/j.algal.2026.104600.

Data availability

Data will be made available on request.

References

[1] B.A. Whitton, M. Potts, Introduction to the cyanobacteria, in: B.A. Whitton (Ed.), Ecology of Cyanobacteria II, Springer, Dordrecht, Netherlands, 2012, pp. 1–13, https://doi.org/10.1007/978-94-007-3855-3_1.
[2] Q. Catherine, W. Susanna, E.-S. Isidora, M. Herrmann, A. Vingiani, J.-F. Humbert, A review of current knowledge on toxic benthic freshwater cyanobacteria: ecology, toxin production and risk management, Water Res. 47 (2013) 5464–5479, https://doi.org/10.1016/j.watres.2013.06.042.
[3] Z. Zahra, D.H. Choo, H. Lee, A. Parveen, Cyanobacteria: review of current potentials and applications, Environments 7 (2020) 13, https://doi.org/10.3390/environments7020013.
[4] R. Hachicha, F. Elleuch, H. Ben Hlima, P. Dubessay, H. de Baynast, C. Delattre, G. Pierre, R. Hachicha, S. Abdelkafi, P. Michaud, I. Fendri, Biomolecules from microalgae and cyanobacteria: applications and market survey, Appl. Sci. 12 (2022) 1924, https://doi.org/10.3390/app12041924.
[5] F. Rossi, R. De Philippis, Exocellular polysaccharides in microalgae and cyanobacteria: chemical features, role and enzymes and genes involved in their biosynthesis, in: M.A. Borowitzka, J. Beardall, J.A. Raven (Eds.), The Physiology of Microalgae, Springer, Cham, Switzerland, 2016, pp. 565–590, https://doi.org/10.1007/978-3-319-24945-2_21.
[6] C. Delattre, G. Pierre, C. Laroche, P. Michaud, Production, extraction and characterization of microalgal and cyanobacterial exopolysaccharides, Biotechnol. Adv. 34 (2016) 1159–1179, https://doi.org/10.1016/j.biotechadv.2016.08.001.
[7] R. De Philippis, M. Vincenzini, Exocellular polysaccharides from cyanobacteria and their possible applications, FEMS Microbiol. Rev. 22 (1998) 151–175, https://doi.org/10.1016/S0168-6445(98)00012-6.
[8] C. Laroche, Exopolysaccharides from microalgae and cyanobacteria: diversity of strains, production strategies and applications, Mar. Drugs 20 (2022) 336, https://doi.org/10.3390/md20050336.
[9] E.E. Andeden, S. Ozturk, B. Aslim, Effect of alkaline pH and nitrogen starvation on the triacylglycerol content, growth, biochemical composition, and fatty acid profile of *Auxenochlorella protothecoides* KP7, J. Appl. Phycol. 33 (2021) 211–225, https://doi.org/10.1007/s10811-020-02311-0.
[10] J. Assunção, H.M. Amaro, T. Tavares, F.X. Malcata, A.C. Guedes, Effects of temperature, pH, and NaCl concentration on biomass and bioactive compound production by *Synechocystis salina*, Life 13 (2023) 187, https://doi.org/10.3390/life13010187.
[11] T.C. Martin, J.T. Wyatt, Comparative physiology and morphology of six strains of stigonematacean blue-green algae, J. Phycol. 10 (1974) 57–65, https://doi.org/10.1111/j.1529-8817.1974.tb02678.x.
[12] F. Rodrigues, I. Mendonça, M. Faria, R. Gomes, J.L.G. Pinchetti, A. Ferreira, N. Cordeiro, Soluble extracellular polymeric substances and microplastics: exposure response and circular reuse for removal, Chemosphere 393 (2025) 144759, https://doi.org/10.1016/j.chemosphere.2025.144759.
[13] M. DuBois, K.A. Gilles, J.K. Hamilton, P.A. Rebers, F. Smith, Colorimetric method for determination of sugars and related substances, Anal. Chem. 28 (1956) 350–356, https://doi.org/10.1021/ac60111a017.
[14] O.H. Lowry, N.J. Rosebrough, A.L. Farr, R.J. Randall, Protein measurement with the Folin phenol reagent, J. Biol. Chem. 193 (1951) 265–275, https://doi.org/10.1016/S0021-9258(19)52451-6.
[15] H.K. Lichtenthaler, Chlorophylls and carotenoids: pigments of photosynthetic biomembranes, Methods Enzymol. 148 (1987) 350–382, https://doi.org/10.1016/0076-6879(87)48036-1.
[16] K. Inoue-Sakamoto, Y. Tanji, M. Yamaba, T. Natsume, T. Masaura, T. Asano, T. Nishiuchi, T. Sakamoto, Characterization of extracellular matrix components

from the desiccation-tolerant cyanobacterium *Nostoc commune*, J. Gen. Appl. Microbiol. 64 (2018) 15–25, https://doi.org/10.2323/jgam.2017.03.001.
[17] K. Stehfest, J. Toepel, C. Wilhelm, The application of micro-FTIR spectroscopy to analyze nutrient stress-related changes in biomass composition of phytoplankton algae, Plant Physiol. Biochem. 43 (2005) 717–726, https://doi.org/10.1016/j.plaphy.2005.07.001.
[18] K. Sudhakar, M. Premalatha, Characterization of microalgal biomass through FTIR/TGA/CHN analysis: application to *Scenedesmus* sp. Energy Sources A: Recovery Util. Environ. Eff. 37 (2015) 2330–2337, https://doi.org/10.1080/15567036.2013.825661.
[19] L. Liu, Q. Huang, Y. Zhang, B. Qin, G. Zhu, Excitation-emission matrix fluorescence and parallel factor analyses of the effects of N and P nutrients on the extracellular polymeric substances of *Microcystis aeruginosa*, Limnologica 63 (2017) 18–26, https://doi.org/10.1016/j.limno.2016.10.006.
[20] L.G. Cardoso, B.B. Andrade, J.S. de Jesus Silva, J.B.A. da Silva, D. de Jesus Assis, N. S. Carvalho, J.C. da Silva, C.O. de Souza, A.T. Lombardi, Effect of nitrate on *Ankistrodesmus fusiformis* culture: evaluation of growth, biomolecules and extracellular polymeric substances (EPS), J. Appl. Phycol. 35 (2023) 1037–1045, https://doi.org/10.1007/s10811-023-02964-7.
[21] S. Kharwar, A. Mukherjee, V. Kumar, E. Shukla, Cyanobacterial stress and its omics perspective, in: B. Neilan, M.R.Z. Passarini, P.K. Singh, A. Kumar (Eds.), Cyanobacterial Biotechnology in the 21st Century, Springer Nature Singapore, Singapore, 2023, pp. 29–50, https://doi.org/10.1007/978-981-99-0181-4_3.
[22] A. Antony, M. Sujitha, T. Rosalin, P.K. Keerthana, W. Wilson, V.T. Anju, Cyanobacterial photosynthetic adaptations in stress environments, in: P.K. Singh, J.S. Panwar, A. Kumar, J. Elster (Eds.), Cyanobacterial Response to Extreme Environments, CABI, Wallingford, UK, 2025, pp. 128–147, https://doi.org/10.1079/9781800623170.0008.
[23] D.K. Saini, S. Pabbi, P. Shukla, Cyanobacterial pigments: perspectives and biotechnological approaches, Food Chem. Toxicol. 120 (2018) 616–624, https://doi.org/10.1016/j.fct.2018.08.002.
[24] M.T. Juergens, R.R. Deshpande, B.F. Lucker, J.-J. Park, H. Wang, M. Gargouri, et al., The regulation of photosynthetic structure and function during nitrogen deprivation in *Chlamydomonas reinhardtii*, Plant Physiol. 167 (2015) 558–573, https://doi.org/10.1104/pp.114.250530.
[25] S. Wang, H. Zhao, D. Qu, L. Yang, L. Zhu, H. Song, H. Liu, Destruction of hydrogen bonding and electrostatic interaction in soy hull polysaccharide: effect on emulsion stability, Food Hydrocoll. 124 (2022) 107304, https://doi.org/10.1016/j.foodhyd.2021.107304.
[26] K. Alba, P.T.M. Nguyen, V. Kontogiorgos, Sustainable polysaccharides from Malvaceae family: structure and functionality, Food Hydrocoll. 118 (2021) 106749, https://doi.org/10.1016/j.foodhyd.2021.106749.
[27] Y. Wang, C. Li, P. Liu, Z. Ahmed, P. Xiao, X. Bai, Physical characterization of exopolysaccharide produced by *Lactobacillus plantarum* KF5 isolated from Tibet kefir, Carbohydr. Polym. 82 (2010) 895–903, https://doi.org/10.1016/j.carbpol.2010.06.013.
[28] J. Wang, X. Zhao, Z. Tian, Y. Yang, Z. Yang, Characterization of an exopolysaccharide produced by *Lactobacillus plantarum* YW11 isolated from Tibet kefir, Carbohydr. Polym. 125 (2015) 16–25, https://doi.org/10.1016/j.carbpol.2015.03.003.
[29] J. Yu, K. Xiao, H. Xu, Y. Li, Q. Xue, W. Xue, A. Zhang, X. Wen, G. Xu, X. Huang, Spectroscopic fingerprints profiling the polysaccharide/protein/humic architecture of stratified extracellular polymeric substances (EPS) in activated sludge, Water Res. 235 (2023) 119866, https://doi.org/10.1016/j.watres.2023.119866.
[30] I. Brezeștean, M. Bocăneală, A.M.R. Gherman, S.A. Porav, I. Kacsó, E. Rakosy-Tican, N.E. Dina, Spectroscopic investigation of exopolysaccharides purified from *Arthrospira platensis* cultures as potential bioresources, J. Mol. Struct. 1246 (2021) 131228, https://doi.org/10.1016/j.molstruc.2021.131228.
[31] X. Zhang, J. Zhao, D.V. Erler, H. Rabiee, Z. Kong, S. Wang, Z. Wang, B. Virdis, Z. Yuan, S. Hu, Characterization of the redox-active extracellular polymeric substances in an anaerobic methanotrophic consortium, J. Environ. Manag. 365 (2024) 121523, https://doi.org/10.1016/j.jenvman.2024.121523.
[32] V. Nóbrega, M. Faria, A. Quintana, M. Kaufmann, A. Ferreira, N. Cordeiro, From a basic microalga and an acetic acid bacterium cellulose producer to a living symbiotic biofilm, Materials 12 (2019) 2275, https://doi.org/10.3390/ma12142275.
[33] D.S.B. Gomes, L.G. Paterno, A.B.S. Santos, D.P.P. Barbosa, B.M. Holtz, M.R. Souza, R.Q. Moraes-Souza, A.V. Garay, L.R. de Andrade, P.P.C. Sartoratto, UV-accelerated synthesis of gold nanoparticle–pluronic nanocomposites for X-ray computed tomography contrast enhancement, Polymers 15 (2023) 2163, https://doi.org/10.3390/polym15092163.
[34] M.S. Aldebasi, H.S. Tar, A.S. Alnafisah, L. Beji, N. Kouki, F. Morlet-Savary, F. M. Alminderej, L.M. Aroua, J. Lalevée, Photochemical synthesis of noble metal nanoparticles: influence of metal salt concentration on size and distribution, Int. J. Mol. Sci. 24 (2023) 14018, https://doi.org/10.3390/ijms241814018.